Access to sodalite cages in ion-exchanged nanosized FAU zeolites probed by hyperpolarized 129Xe NMR and DFT calculations

Eddy Dib, Jérôme Rey, Aurelie Vicente, Shrikant Kunjir, Hussein Awala, Sarah Komaty, Ayoub Daouli, Tomáš Bučko, Hussein El Siblani, Robert Bedard, et al.

Access to sodalite cages in ion-exchanged nanosized FAU zeolites probed by hyperpolarized ^{129}Xe NMR and DFT calculations

Eddy Dib[1],* Jérôme Rey[2], Aurelie Vicente[1], Shrikant Kunjir[1], Hussein Awala[1], Sarah Komaty[1], Ayoub Daouli[2], Tomáš Bučko[3,4], Hussein El Siblani[1], Robert Bedard[5], Jeffery Bricker[5], Jean-Pierre Gilson[1], Michael Badawi[2], Svetlana Mintova[1]*

[1]Laboratoire Catalyse et Spectrochimie (LCS), Normandie Université, ENSICAEN, UNICAEN, CNRS,6 boulevard du Maréchal Juin, 14050 Caen, France.

[2]Laboratoire de Physique et Chimie Théoriques, UMR 7019 – CNRS, Université de Lorraine, F-54000 Nancy, France.

[3]Department of Physical and Theoretical Chemistry, Faculty of Natural Sciences, Comenius University in Bratislava, SK-84215 Bratislava, Slovakia.

[4]Institute of Inorganic Chemistry, Slovak Academy of Sciences, SK-84236 Bratislava, Slovakia.

[5]UOP LLC, Des Plaines, Illinois 60016, United States.

Corresponding authors: eddy.dib@ensicaen.fr; svetlana.mintova@ensicaen.fr

Abstract

The accessibility to sodalite (SOD) cages in nanosized zeolite X (FAU-type framework) is tuned by varying the nature and location of extra-framework exchangeable cations (Na^+, Li^+, Cs^+, K^+ and Rb^+). Hyperpolarized (HP) and EXchange SpectroscopY (EXSY) ^{129}Xe NMR experiments highlight the connectivity between SOD- and super (SUP)-cages, in particular that its diffusion pathway from sodalites to supercages depends mainly on the size and location of extra-framework cations present in the zeolite. These ^{129}Xe NMR results are supported by DFT simulations. Based on the computed adsorption energies of Xe in both SOD and SUP cages of zeolite X with different cationic compositions, it is concluded that xenon penetration in SUP cages is always favorable while the adsorption in the SOD cages is possible only if small cations (Na^+, Li^+, K^+) are present.

Introduction

Zeolites are crystalline microporous aluminosilicates widely used in industry[1,2,3] and among their many interesting features, the capacity to exchange their extra-framework cations is the key to their superior performances in applications such molecular separations, depollution and catalysis.[4] The Faujasite (FAU) type zeolite is one of the most widely used,[5,6,7] due to the shape selectivity of the framework structure and its ability to adopt variable chemical compositions.[8] The FAU structure has a pore opening of 0.74 nm and contains two types of cages : (i) sodalite cages (SOD) with an inside diameter of 0.63 nm and (ii) supercages with a diameter of 1.12 nm, interconnected by hexagonal six membered ring windows of 0.23 nm. The supercages are known to be accessible to many molecules through 12 membered ring windows with a diameter of 0.73 nm (Supporting Information, Figure S1). The sodalite cages contain a high proportion of active sites (almost 60%), which are, unfortunately, not accessible.[9] This is due to the small size of the six membered ring windows connecting the cages to their vicinity.[10]

The ^{129}Xe (nuclear spin I = ½, 26.44 % natural abundant) is an excellent NMR probe for porous materials as its chemical shift is very sensitive to the dimensions of their cavities, channels and the nature of their adsorption sites. Its hyperpolarization (HP) substantially increases sensitivity and is becoming a powerful technique to characterize zeolites in particular[11]. Thermal ^{129}Xe is already used routinely to analyze zeolites porosity and connectivity.[12] The increased sensitivity of HP ^{129}Xe NMR for instance, allows to monitor the recrystallization of a tiny amount of MFI zeolite on hierarchical BEA zeolite walls. More specifically, the role of tetrapropylammonium cations in preventing extensive amorphization of BEA zeolites during the alkaline leaching produces homogeneously distributed mesopores with the coexistence of both zeolites at the interface.[13]

In micron-sized FAU zeolites, Xe accesses only the supercages as its kinetic diameter (~ 0.39 nm) is larger than the six membered ring windows leading to SOD cages.[14] The opening of SOD cages in a Y-type FAU zeolite was reported during its hierarchization using the unbiased NH_4F demetallation procedure[15]. A ^{129}Xe NMR peak observed at a higher chemical shift (~ 110 ppm) than the peak corresponding to the SUP (~ 75 ppm) was attributed to Xe in SOD cages, in agreement with other experimental proofs. Their interconnectivity and the formation of mesopores was further investigated in a recent study using HP ^{129}Xe NMR, high resolution transmission electron microscopy (HRTEM) and density functional theory (DFT)

calculations[16]. During the unbiased etching, the removal of tetrahedral atoms from the framework, led to the opening of some SOD cages and connections between neighboring sodalite and supercages. A new and fast diffusion pathway where Xe first diffuses from opened SOD to SUP of the FAU zeolite was proposed. Superior catalytic performances resulted due to the availability of more active sites and reduced transport limitations in the hierarchical zeolite crystals. In another study on the crystallization kinetics of ultra-small FAU-type zeolite crystals, the formation of the first micropores and the occurrence of opened SOD cages was confirmed by HP ^{129}Xe NMR spectroscopy[17].

However, the amount and location of alkali cations of different sizes may influence the diffusional pathway of guest molecules, the cages' accessibility, and consecutively, the corresponding catalytic activity of nanosized FAU zeolites. Studying the effect of alkali cations location on the diffusion pathway is then a very important step allowing to tune the zeolites properties. In the present work, nanosized FAU zeolites prepared with different alkali cations are investigated using *inter alia* hyperpolarized ^{129}Xe NMR spectroscopy and DFT calculations in order to better understand the effect of these cations on the accessibility of the SOD cages.

Experimental section

Synthesis

A parent nanosized (10-15 nm) Na-FAU zeolite (type X with Si/Al ratio of 1.1) was synthesized from a transparent precursor suspension (composition: $9Na_2O$: $1.1Al_2O_3$: $10SiO_2$: $50H_2O$) first aged at ambient temperature for 24 h and thereafter heated in an autoclave at 323 K for 26 h. The nanocrystals harvested were washed by double distilled water and the crystals were collected by a high-speed centrifuge and then re-dispersed in H_2O. The process was repeated until a pH of 8 of the decant was reached. The as-synthesized zeolite (Na-X) was then ion-exchanged with Li, K, Rb and Cs salts. Typically, 1.0 g of zeolite powder was stirred in 35 mL of nitrate solutions of the targeted cations with concentrations of 0.2 M for Li and K and 0.005 M for Rb and Cs. The ion-exchanged samples were abbreviated Li-X, K-X, Rb-X and Cs-X. The difference in concentration was applied to preserve the zeolite structure and avoid amorphization of the zeolite nanocrystals. The exchange process was repeated three times by separating supernatant from mother liquid, re-dispersing in new nitrate solution, and carrying on with the aforementioned ion exchange process to ensure that

the highest possible ion exchange was achieved. The samples after ion-exchanged were washed thoroughly with double distilled water (pH = 7.5) and subjected to freeze-drying.

Characterization

The X-ray diffraction (XRD) patterns of zeolite samples were recorded using a PANalytical X'Pert PRO XRD diffractometer. The morphology of the as-synthesized and ion-exchanged zeolite nanocrystals was evaluated by field emission scanning electron microscope (FE-SEM) using a JEOS JSM6700F SEM with an accelerating voltage of 30 kV. The porosity of the samples was determined by nitrogen sorption with a Micromeritics ASAP 2010 instrument.

^{29}Si, ^{23}Na, and ^{27}Al MAS NMR spectra of zeolite samples were recorded using a Bruker Avance III 400 MHz spectrometer. For ^{29}Si MAS NMR, 2 μs pulse (π/6) was used with a recycle delay of 15 s. For ^{23}Na and ^{27}Al MAS NMR spectra, radiofrequency pulses of 1.60 and 1.67 μs (π/8), were used with 0.5 s and 1 s of recycle delay, respectively. Tetramethylsilane (TMS), sodium chloride (NaCl 0.1 M) and (aluminum nitrate, Al $(NO_3)_3$, 0.1M) were used as references for ^{29}Si, ^{23}Na, and ^{27}Al chemical shifts respectively.

Continuous flow ^{129}Xe HP NMR experiments were performed at 110.6 MHz in a Bruker Avance III-HD 400 (9.4 T) spectrometer using a 10 mm BBO probe. The one-dimensional HP ^{129}Xe NMR spectra were recorded with 128 scans using a single 90° excitation pulse with a length of 12.5 μs and a recycle delay of 1 s. The HP ^{129}Xe was produced in a home-built xenon polarizer based on the Spin-Exchange Optical Pumping (SEOP) technique, capable of delivering a continuous flow of HP- ^{129}Xe directly to the sample inside the NMR spectrometer. Before each experiment, all samples were compressed into pellets under a 100 MPa pressure, then crushed and sieved and the 200-500 μm fraction retained. 0.5 g of zeolite was introduced into 10 mm NMR tube and dehydrated under high-vacuum (10^{-6} mbar) at 548 K overnight. ^{129}Xe NMR spectra were acquired under continuous recirculating flow at 50 mL·min^{-1} of a gas mixture containing 90% He, 6% N_2, and 4% of natural abundance Xe at a pressure of 0.15 MPa. For all variable temperature measurements and after each temperature change performed at a speed of 5 K·min^{-1}, a delay of about 20 min was applied to ensure a homogeneous temperature all over the samples; the stability was checked by monitoring the ^{129}Xe chemical shifts. 2D exchange spectroscopy (EXSY) HP ^{129}Xe NMR spectra were recorded using a basic three pulses sequence.

Computational details

DFT calculations

Periodic DFT calculations were performed using the VASP (Vienna Ab initio Simulation Package) code.[18,19] A plane-wave basis set was used with cutoff energies of 400 eV for the relaxation of atomic positions and 1050 eV for cell relaxations within the projector augmented wave (PAW) method of Blöchl,[20] as adapted by Kresse and Joubert[21] and with a Gaussian smearing of 0.05 eV. As a large supercell was employed in calculations (see the structural model below), the Brillouin zone sampling was restricted to the Γ–point.

The semi-local exchange correlation functional PBE was employed.[22] Since the dispersion interactions, important to describe ^{129}Xe adsorption in a zeolite, are not correctly described by this method, we have used the TS/HI correction scheme[23] which is an accurate variant ot the Tkatchenko-Scheffler dispersion correction improved with iterative Hirshfeld partitioning.[24,25] The TS/HI scheme is particularly well suited for the description of ionic systems such as cationic zeolites.[26,27,28] The convergence criterion for the electronic self-consistency cycle was set to 10^{-7} eV. Structural relaxations were carried out with a conjugate-gradient algorithm[29] until all forces were smaller than 0.01 eV/Å.

The adsorption energy of Xe in different cages of cationic exchanged FAU zeolites were computed with the following equation:

$$\Delta E = E_{Xe@FAU} - E_{Xe} - E_{FAU}, \quad (1)$$

where $E_{Xe@FAU}$ is the electronic energy of adsorbed Xe in the cage of FAU zeolite, E_{Xe} is the energy of Xe in the gas phase and E_{FAU} is the energy of an empty FAU zeolite.

Structural models used in DFT calculations

The primitive cells of X zeolite (FAU zeolite with a Si/Al ratio higher than 1) were prepared whereby 22 out of the 48 silicon atoms of FAU zeolite were substituted by aluminium atoms and 22 extra-framework alkaline cations were added to create the Li-X, Na-X and K-X structures (Si/Al ratio of 1.18). These primitive cells were fully optimized, with relaxation of the atomic positions and of the cell shape and volume. The four (I') sites of sodalite cages are occupied by extra-framework cations, as described in the review of Frising and Leflaive.[30] The cell parameters and the structure of the supercage and the sodalite cage of Na-X are reported in SI (Table S1 and Figure S1).

To match the real samples' compositions in the theoretical calculations, especially for the Rb-X and Cs-X variants with big molar percentage of sodium ions among extra-framework cations (around 50 % for Rb-X and 25 % for Cs-X, see **Table 1**), we prepared cells with different ratios of substitutions of Na by Rb or Cs in the cages occupied by the Xe atom. The corresponding cells are denoted $Na_{0.75}Rb_{0.25}X$ and $Na_{0.50}Rb_{0.50}X$ (and similarly for Cs), when one or two out of the four extra-framework Na cations closest to Xe atom are replaced by Rb or Cs. In the sodalite cage, four extra-framework Na cations per cage are equivalent (site I'), giving only one structure for $Na_{0.75}Rb_{0.25}X$ and $Na_{0.50}Rb_{0.50}X$ and similar structures are used for the Cs-X. In the supercage, the two closest Na atoms occupying sites II and III were substituted for $Na_{0.75}Rb_{0.25}X$, opening two possibilities, and two of the four closest extra-framework cations were substituted to prepare of $Na_{0.50}Rb_{0.50}X$, giving thus four different structures. Same structures were obtained for Cs-X. These different permutations of the Rb/Na and Cs/Na were taken into account to describe the statistical diversity of environments of the experimental samples. According to the extra-framework cation distribution reported in Leflaive's review[29] we used in the case of K-X a structure with three extraframework K cations in the sodalite cage, the fourth one being displaced into the site I (consistently, it was not possible to optimize the structure with Xe adsorbed in the SOD cage with 4 extra-framework K^+).

Results and discussion

The X-ray diffraction patterns of all zeolites indicate a high degree of crystallinity and phase purity unchanged after ion exchange (**Figure 1**).

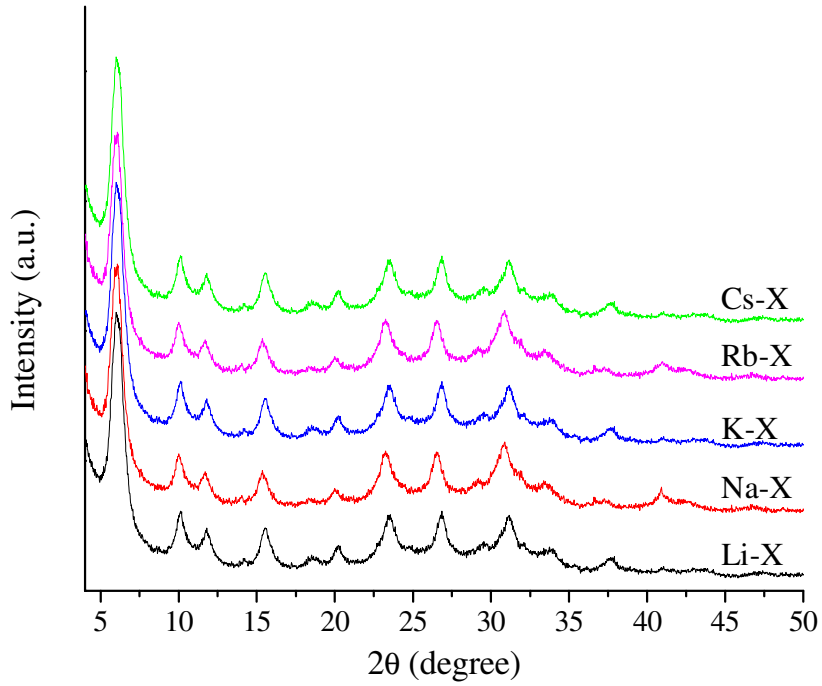

Figure 1. XRD patterns of nanosized Li-X (black), Na-X (red), K-X (blue), Rb-X (pink) and Cs-X (green) zeolite samples. All Bragg peaks in the patterns correspond to the FAU type zeolites[31].

The size and morphology of the nanosized zeolite crystals after ion exchange with Li, Na, K, Rb, and Cs are fully preserved (SI, Figure S2). The zeolite nanocrystals remain stable after ion exchange, and no agglomeration occurs. FE-SEM shows zeolites crystals with a mean size of 15 nm with a narrow particle size distribution. All zeolites have the same Si/Al ratio of ~1.1. After three ion exchanges of the parent nanosized zeolite (Na-X), the following exchange degrees are achieved: Li^+ (79.7%), K^+ (88.7%), Rb^+ (53.3%) and Cs^+ (26.5%). Their framework Si/Al ratio determined by ^{29}Si NMR are summarized in **Table 1**.

Table 1. Framework Si/Al ratio of as-synthesized and ion-exchanged zeolites determined by ^{29}Si NMR; the amount of Na remaining in the samples determined by ^{23}Na MAS NMR (the as-synthesized Na-X is used as a reference sample).

Sample	Si/Al	Sodium (%)
Na-X	1.06	100.0
Li-X	1.06	20.3
K-X	1.12	11.3
Rb-X	1.14	46.7
Cs-X	1.13	73.5

All samples exhibit Type I isotherms at low N_2 P/P_0, characteristic of microporous materials (**Figure 2**). Another uptake at $P/P_0 > 0.8$ is due to the textural mesoporosity resulting from the close packing of zeolite nanoparticles on all samples. The N_2 uptake at low P/P_0 is inversely proportional to the size of cations (SI, Table S2), *i.e* Li-X exhibits the highest micropore volume (V_{micro}), whereas Cs-X zeolite shows the lowest microporosity.

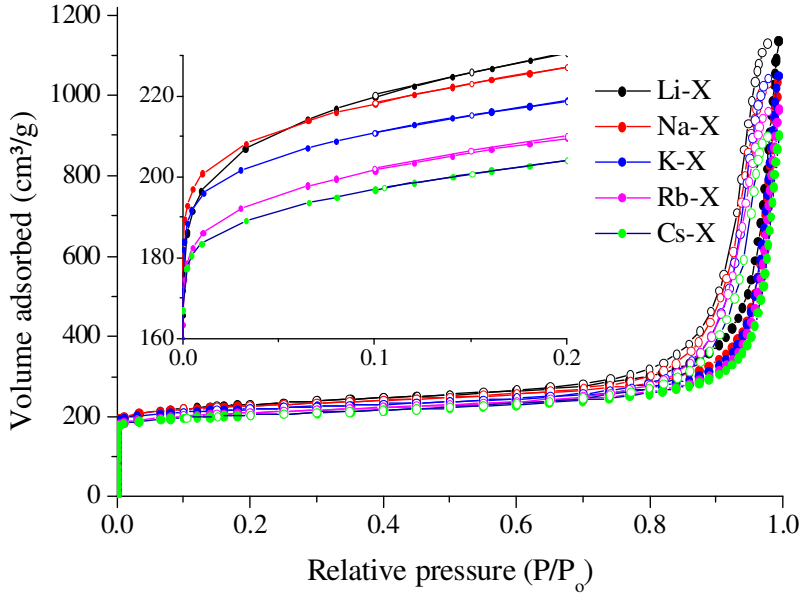

Figure 2. N_2 adsorption (open circles) and desorption (full circles) isotherms of Li-X (black), Na-X (red), K-X (blue), Rb-X (pink) and Cs-X (green) zeolite nanocrystals.

Figures S3 and S4 indicate the local order of all zeolites is mainly unchaged during the ion-exchanges. Their ^{27}Al MAS NMR spectra contain only one peak at ~60 ppm corresponding to the tetrahedral aluminum. The ^{29} Si MAS spectra show well-resolved spectra with two main peaks at -85 ppm corresponding to $Q^4(4Al)$ and at -89 ppm corresponding to $Q^3(3Al)$. These results are in a good agreement with previously reported data on zeolite X with a Si/Al ratio of 1.[32]

HP ^{129}Xe NMR experiments were performed to identify the possible adsorption sites and diffusion pathways of Xe in the nanosized zeolite samples containing various extra-framework cations with different sizes. Continuous flow HP ^{129}Xe NMR experiments are performed at different temperatures (250 - 370 K). The HP ^{129}Xe NMR spectra recorded at 300 K are depicted in Figure 3. The peak of ^{129}Xe in the gas is used as the reference and set at 0 ppm. Two peaks (~ 80 and ~ 90 ppm) are observed on Li-X, Na-X, and K-X zeolites, but a single peak on Rb-X (89.5 ppm) and Cs-X (96.2 ppm). When two peaks are present, they are

assigned to Xe located SOD cages (highest chemical shift) and SUP cages (lowest chemical shift)[15]. The difference in chemical shift is mainly due to the difference in the size of the SOD and SUP cavities[3334]. This indicates that SOD and SUP cages are both accessible when small cations are present (Li, Na, and K), while only the SUP is accessible to xenon when the bulkier cations (Rb and Cs) are present.

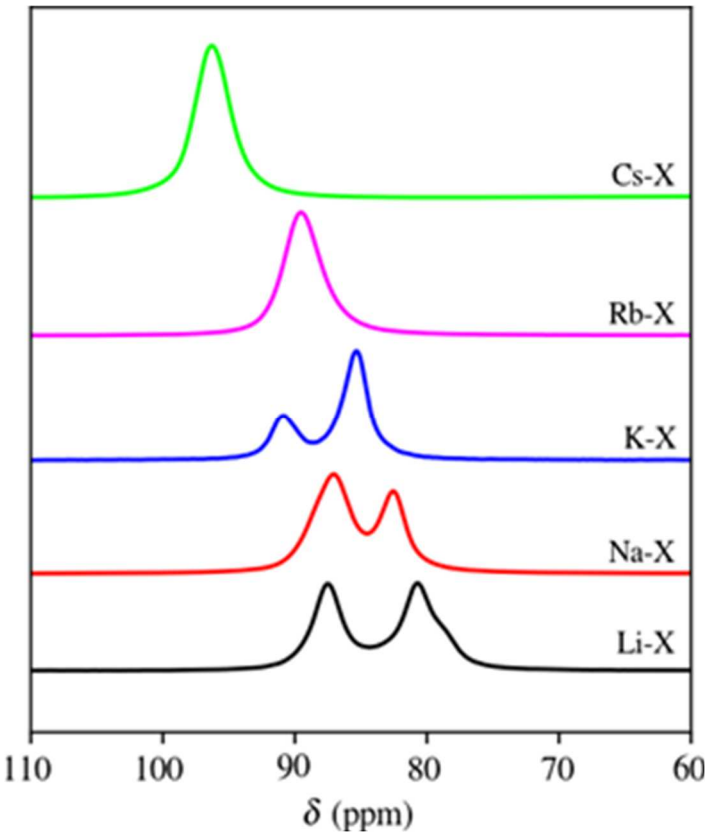

Figure 3. 1D HP ^{129}Xe NMR spectra of nanosized Li-X (black), Na-X (red), K-X (blue), Rb-X (pink) and Cs-X (green) zeolite samples recorded at 300 K. Zeolites Li-X, Na-X and K-X present two peaks corresponding to SOD cages (high chemical shift) and SUP cages (low chemical shift) while zeolites Rb-X and Cs-X show only one peak corresponding to SUP cages.

Xe atoms may have several scenarios for the exchange between the gas phase and the adsorption sites or between different adsorption sites with different sizes. It is important to indicate whether gas phase xenon accesses the SUP via the SOD or follows a different pathway. This information can be obtained from the exchange rates between different phases or cavities[35]. When two different sites are present and if the Xe exchange rate is faster than the NMR time scale, a single resonance with weighted average shift will appear, a phenomenon named coalescence. However, if the exchange rate is slower than the NMR time

scale, two peaks will appear. Reducing the temperature of the measurement and therefore the exchange rate(s), allows to better distinguish between the above scenarios[36]. Our results at different temperatures are summrazied in **Table 2**. Below 330 K, Li-X, Na-X and K-X contain two peaks corresponding to two environments while Rb-X and Cs-X present one peak even at 250 K. This result clearly demonstrate a single environment for Xe in Rb-X and Cs-X zeolites.

Table 2. Isotropic chemical shift of ^{129}Xe in Li-X, Na-X, K-X, Rb-X and Cs-X zeolite nanocrystals at different temperatures.

	Li-X		**Na-X**		**K-X**		**Rb-X**		**Cs-X**	
T (K)	Super	SOD	Super	SOD	Super	SOD	Super	SOD	Super	SOD
370	68.1	---	72.2	---	70.9	---	72.4	---	80.6	---
350	71.4	78.3	74.9	---	74.9	---	76.6	---	85.3	---
330	74.9	81.8	77.7	81.7	79.1	84.7	81.8	---	89.7	---
310	---	---	80.8	85.4	83.3	88.5	87	---	94.1	---
300	80.7	87.5	82.5	87	85.3	90.9	89.5	---	96.2	---
290	82.6	89.1	84.2	88.7	86.9	92.5	91.3	---	97.6	---
270	86.9	92.6	88.1	92.2	91.5	96.4	96.2	---	101.1	---
250	91.3	96.7	94.1	97.3	98.7	102.3	101.8	---	105.3	---

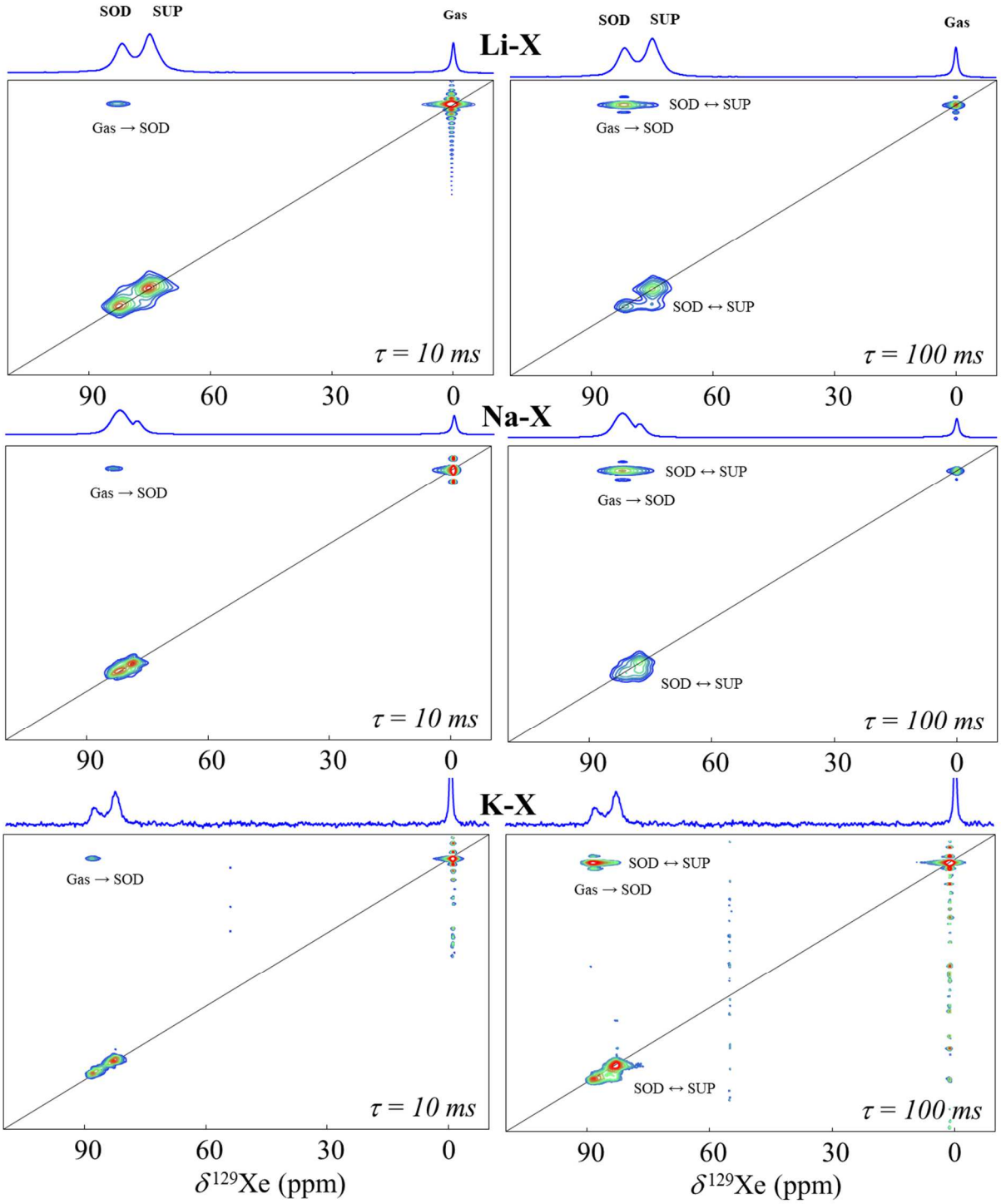

Figure 4. 2D EXSY HP ^{129}Xe NMR spectra of nanosized Li-X and Na-X and K-X zeolite samples recorded at 330 K at mixing time of 10 ms (left spectra) and at100 ms (right spectra).

The interconnectivity of the cages in the nanosized FAU zeolites containing different cations is probed using ^{129}Xe 2D exchange spectroscopy (EXSY). This 2D experiment measures the extent of chemical exchange between Xe adsorbed in different pores or cages and gas phase Xe. These ^{129}Xe 2D spectra exhibit two types of cross peaks: i) along the diagonal: Xe in

pores with different sizes, ii) off-diagonal cross-peaks: Xe exchanges between pores during a given exchange or a mixing time. The 2D EXSY HP ^{129}Xe NMR spectra recorded for nanosized Li-X, Na-X and K-X zeolite samples at 330 K with a short (10 ms) and a long (100 ms) mixing times are depicted in **Figure 4.** The diagonal peaks at (0; 0), (75; 75), and (81; 81) ppm in the spectra are attributed to the xenon in gas phase, supercages, and sodalite cages respectively (see **Figure 4**). Additionally, cross peaks appear in the 2D spectra, revealing chemical exchanges. Interestingly, the Xe atoms directly go from gas to SOD cages and not through the supercages (see the (81; 0) cross peak). Additionally, an exchange occurs between Xe in SOD and supercages and vice versa at longer mixing times (Figure 4, right spectra). This proves that the xenon diffuses through the SOD cages via the opened six membered ring windows to the supercages. These observations are in line with previous studies revealing the diffusion of Xe into the opened SOD cages before diffusing to the SUP of nanosized FAU zeolites[15-17]. The Xe atoms are not accessing the SOD cages through the supercages and these SOD cages are accessible only for the samples Li-X, Na-X and K-X and not accessible for the Rb-X and Cs-X samples. Apparently, the presence of big cations (Rb and Cs), blocks the access to SOD cages so that they can not accomodate the Xe atoms. This result shows that Rb and Cs cations are located somewhere at the opening of the SOD cages and the exchange of Na in the SOD cages for other cations is possible. Note that the EXSY spectra are not symmetric as expected due to the loss of Xe polarization after interacting with the zeolite pore walls.

DFT calculations

Adsorption energies of xenon in supercages and SOD cages were computed using Eq. (1) for zeolite X containing different cations. The results are shown in **Figure 5** and Table S3. Some relevant optimized structures of Na-X and Cs-X zeolites are shown in **Figure 6**. The adsorption of xenon in supercages is always favorable (negative adsorption energy), with only a small effect of the nature of the extraframework cation. In the sterically constrained sodalite cage, in contrast, the adsorption becomes endothermic when the large extraframework cations (Rb^+ and Cs^+) are present. This observation is not dependent on the ratio of substitution of Na^+ by the large cations (Rb^+ or Cs^+). As shown in Table S3, the dispersion contribution to the electronic energy of adsorption is always favorable, whereas the steric repulsion increases in sodalite cages for the samples containing Cs and Rb cations, leading to an unfavorable adsorption. Thus, the DFT results strongly support the experimental

conclusion that Xe is unlikely to be located in sodalite cages in the case of the Rb-X and Cs-X zeolite samples.

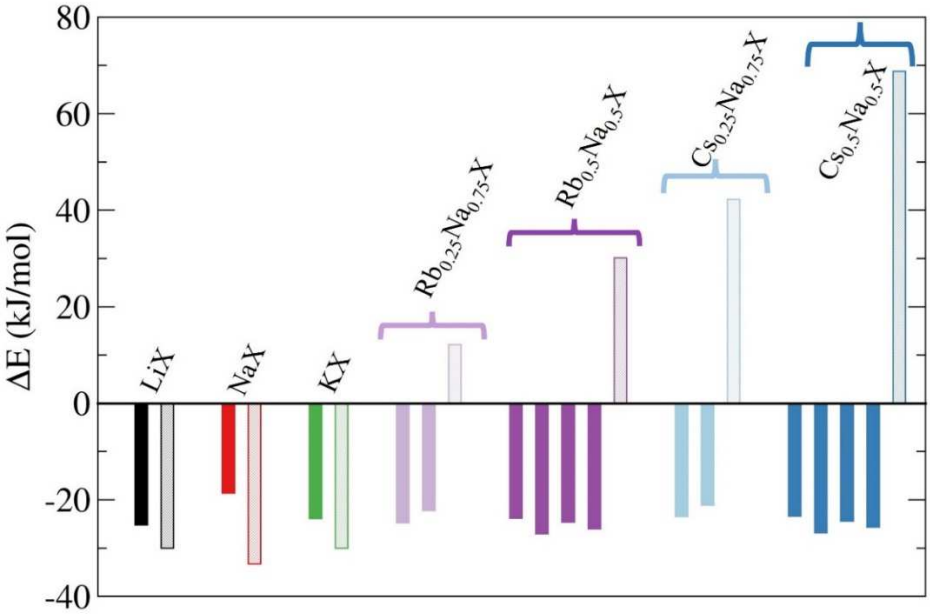

Figure 5. Electronic energies of adsorption (ΔE) of xenon in supercage (full bars) and sodalite cages (hatched bars) of zeolite X containing different cations.

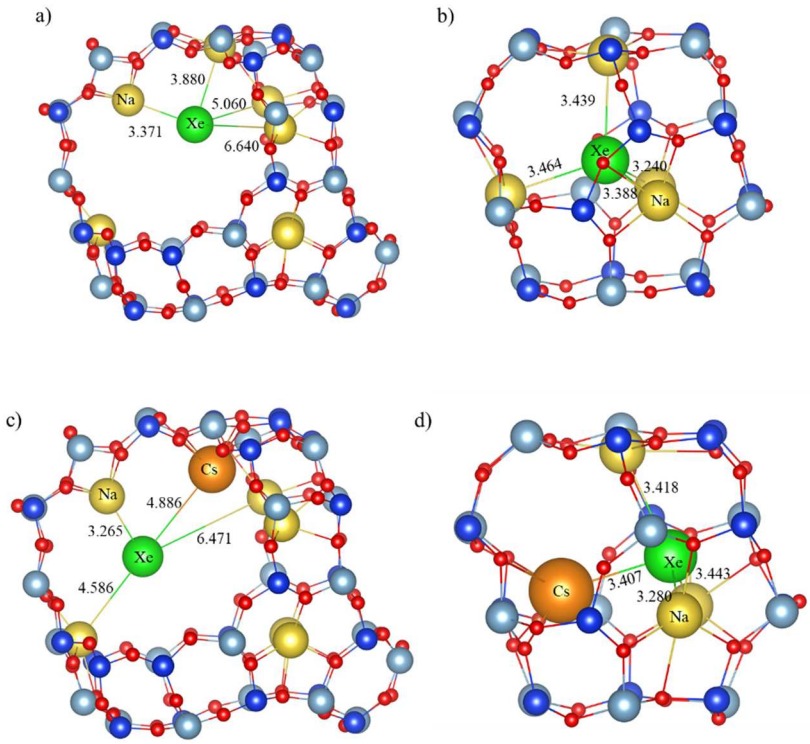

Figure 6. Optimized structures for xenon atom adsorbed in the supercage (a) and sodalite cage (b) of Na-X zeolite, and in the supercage (c) and sodalite cage (d) of Cs-X zeolite. Color code: Xe (green), Na (yellow), Cs (orange), Si (blue), Al (light blue), O (red). The four shortest distances Xe-alkaline cations are reported in Å.

Conclusions

In this work, we have shown how the accessibility to SOD cages in nanosized FAU type X zeolites (Si/Al ratio of 1.2) can be controlled by varying the type and location of extra-framework exchangeable cations. Hyperpolarized (HP) and EXchange SpectroscopY (EXSY) ^{129}Xe NMR experiments showed the connectivity between the cages and confirmed that the pathway from sodalite to supercages is only possible when small cations like Na^+, Li^+ and K^+ are present while this is not observed in the case of Rb^+ and Cs^+ exchanged zeolite samples. The experimental observations are supported by DFT calculations revealing the adsorption energies of Xe in sodalite and supercages with different statistical distributions of cations. Accomodation of Xe in supercages is always energetically favorable for all alkali metal cations. In contrast, Xe adsorption is exothermic only in sodalite cages which contain small cations (Li^+, Na^+ and K^+). These results strongly support the experimental finding based on ^{129}Xe NMR that Xe does not enter the sodalite cages of RbX and CsX zeolites. This work paves the way for the development of nanosized zeolites containing different cations for optimized applications in adsorption and catalysis.

Acknowledgments

We acknowledge the support of the UOP-Honeywell, Label of Excellence for the Centre for zeolites and nanoporous materials by the Region of Normandy (CLEAR). This work was granted access to the HPC resources of TGCC under the allocation 2021-A0100810433 by GENCI-EDARI project. JR and MB thank Ioannis Karamanis (Université de Lorraine) for fruitful discussions. JR and MB also acknowledge the financial support of the COMETE project (COnception in silico de Matériaux pour l'EnvironnemenT et l'Energie) cofounded by the European Union under the program "FEDER-FSE Lorraine et Massif des Vosges 2014-2020". TB is grateful to the Slovak Research and Development Agency under the contract No. VEGA-1/0777/19 and APVV-20-0127 for the support.

References

[1]E.M Flanigen, R.W. Broach, S. T. Wilson, in Zeolites in Industrial Separation and Catalysis; S. Kulprathipanja, Ed.; Wiley-VCH: Weinheim, (2010) 1– 26.
[2] W. Vermeiren, J.-P. Gilson, Top. Catal. 52, (2009), 1131– 1161.
[3]S. Komaty, A. Daouli, M. Badawi, C. Anfray, M. Zaarour, S. Valable and S. Mintova, Phys. Chem. Chem. Phys., 22, (2020), 9934–9942.
[4]S. Ernst, Angew. Chemie Int. Ed., 50, (2011), 5425–5426.
[5]I. Braschi, S. Blasioli, L. Gigli, C. E. Gessa, A. Alberti and A. Martucci, J. Hazard. Mater., 178, (2010), 218–225.
[6]S. Komaty, H. Özçelik, M. Zaarour, A. Ferre, S. Valable and S. Mintova, J. Colloid Interface Sci., 581, (2021), 919–927.
[7]H. Awala, J. P. Gilson, R. Retoux, P. Boullay, J. M. Goupil, V. Valtchev and S. Mintova, Nat. Mater., 14, (2015), 447–451.
[8]H. Hattori and Y. Ono, in Metal Oxides in Heterogeneous Catalysis, Elsevier, (2018), 133 – 209.
[9]H. An, S. Kweon, S. Park, J. Lee, H. K. Min and M. B. Park, Nanomaterials, 10, (2020), 1– 13.
[10]H. G. Karge, M. Hunger and H. K. Beyer, in Catalysis and Zeolites, Springer Berlin Heidelberg, (1999), 198–326.
[11]A. Nossov, E. Haddad, F. Guenneau, A. Gedeon, Phys. Chem. Chem. Phys., 5(20), (2003), 4479-4483.
[12]J. L. Bonardet, J. Fraissard, A. Gédéon and M. A. Springuel-Huet, Catal. Rev. Sci. Eng., 41, (1999), 115–225.
[13]E. Dib, H. El Siblani, S. M. Kunjir, A. Vicente, N. Nuttens, D. Verboekend, B. F. Sels, C. Fernandez, Cryst. Growth Des. 18(4), (2018), 2010–2015.
[14]P. J. Barrie, J. Klinowski, Progress in NMR Spectroscopy, 24, (1992), 91-108.
[15]Z. Qin, K. A. Cychosz, G. Melinte, H. El Siblani, J. P. Gilson, M. Thommes, C. Fernandez, S. Mintova, O. Ersen and V. Valtchev, J. Am. Chem. Soc., 139, (2017), 17273–17276.
[16]Z. Qin, S. Zeng, G. Melinte, T. Bučko, M. Badawi, Y. Shen, J-P. Gilson, O. Ersen, Y.Wei, Z. Liu, X. Liu, Z. Yan, S. Xu, V. Valtchev, S. Mintova , Adv. Sci., 8, (2021), 2100001, 1-9.
[17]H. Awala, S. M. Kunjir, A. Vicente, J-P Gilson, V. Valtchev, H. El Siblani, R. Retoux, L. Lakiss, C. Fernandez, R. Bedard, S. Abdo, J. Bricker, S. Mintova, J. Mater. Chem. A, 9, (2021), 17492-17501.
[18]G. Kresse, J. Hafner, Phys. Rev. B 47, (1993), 558-561.
[19]G. Kresse, J. Hafner, Phys. Rev. B 49, (1994), 14251-14269.
[20]P. E. Blöchl, Phys. Rev. B 50, (1994), 17953-17979.
[21]G. Kresse, D. Joubert, Phys. Rev. B, 59, (1999), 1758-1775.
[22]J. P. Perdew, K. Burke, M. Ernzerhof, Phys. Rev. Lett. 77, (1997), 3865-3868.
[23]T. Bučko, S. Lebègue, J. G. Ángyán, J. Hafner, J. Chem. Phys. 141, (2014), 034114, 1-17.
[24]A. Tkatchenko, M. Scheffler, Phys. Rev. Lett. 102, (2009), 073005, 1-4.
[25]N. Marom, A. Tkatchenko, M. Scheffler, L. Kronik, J. Chem. Theory Comput. 6(1), (2010), 81–90.
[26]H. Jabraoui, I. Khalil, S. Lebègue, M. Badawi, Mol. Syst. Des. Eng., 4, (2019), 882-892.
[27]E. P. Hessou, W. G. Kanhounnon, D. Rocca, H. Monnier, C. Vallières, S. Lebègue, M. Badawi, Theoretical Chemistry Accounts, 137 (2018), 161-173.
[28]S. Chibani, M. Chebbi, S. Lebègue, T. Bučko, M. Badawi, J. Chem. Phys. 144, (2016), 244705, 1-10.

[29]Numerical Recipes in FORTRAN (2nd Ed.), The Art of Scientific Computing, Cambridge University Press, New York, NY, USA, 1992.
[30]T. Frising, P. Leflaive, Micropor. Mesopor. Mater, 14, (2008), 27-63.
[31] Baur, W.H. Am. Mineral., 49, (1964), 697-704.
[32]T. Melchior, D. E. W. Vaughan, C. F. Pictroski, J. Phys. Chem. 99, (1995), 99, 6128-6144.
[33] J. Fraissard, T. Ito, Zeolites, 8, (1988), 350-361.
[34] M-A Springuel-Huet, J-L. Bonardet, A. Gedeon, J. Fraissard, Magn. Reson. Chem., 37, (1999); S1–S13.
[35] I.L. Moudrakovski, L.Q.Wang, T. Baumann, J. H. Satcher, G. J. Exarhos, C.I. Ratcliffe, J.A. Ripmeester, J. Am. Chem. Soc., 126(16), (2004), 5052-5053.
[36] H.S. Gutowsky, H. N. Cheng, J. Chem. Phys. 63, (1975), 2439-2441.

ΔE_{ads} = +40 kJ.mol^{-1}

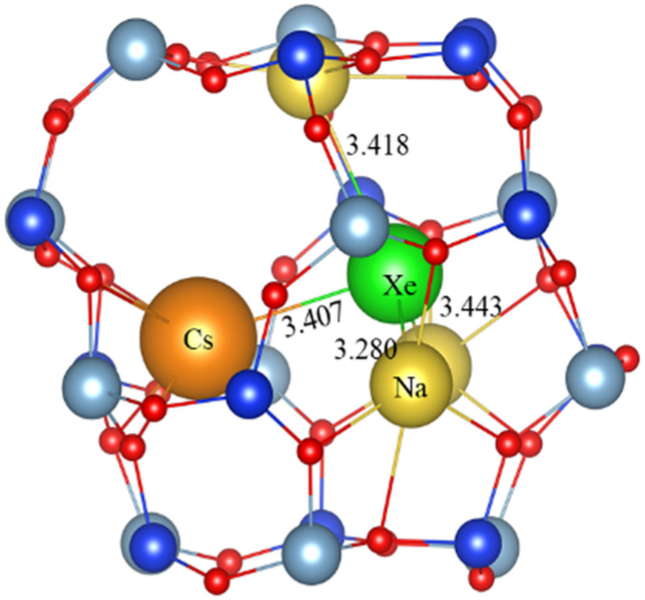

Cs-X

ΔE_{ads} = -30 kJ.mol^{-1}

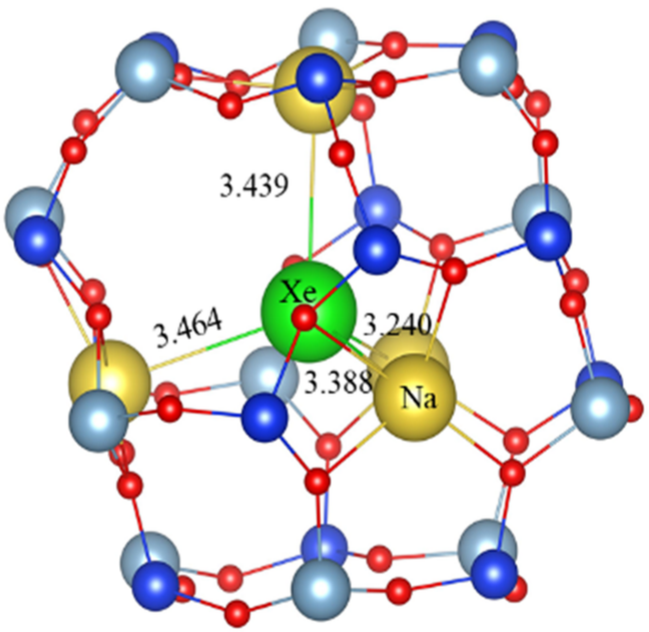

Na-X

110 100 90 80 70 60

δ^{129}Xe (ppm)